

## Experimental and Theoretical Studies of Electron-Impact Excitation of Neon\*

Francis A. Sharpton

*Olivet Nazarene College, Kankakee, Illinois 60901*

and

Robert M. St. John

*Department of Physics and Astronomy, University of Oklahoma, Norman, Oklahoma 73069*

and

Chun C. Lin

*Department of Physics, University of Wisconsin, Madison, Wisconsin 53706*

and

Fredric E. Fajen

*Los Alamos Scientific Laboratory, Los Alamos, New Mexico 87544*

(Received 27 February 1970)

The electron excitation functions of some fifty states from the  $2p^5ns$ ,  $2p^5np$ , and  $2p^5nd$  configurations have been measured by the optical method. Corrections due to cascade from the upper levels are important only for the  $np$  states and typically amount to 50% of the total population. The scheme of characterizing the excitation behaviors of helium by the quantum numbers  $L$  and  $S$  of the states can be carried over to neon if one expresses the wave functions of the excited states of neon in terms of the  $LS$  eigenfunctions. For example, all the optically allowed states exhibit very broad excitation functions and large cross sections, and the purely triplet states have narrow excitation functions. For the other states, the wave functions are expressible as linear combinations of those of triplet states and dipole-forbidden singlet states; hence, the excitation functions have intermediate widths. From group-theoretical arguments, we have shown that within a configuration  $2p^5nl$ , the states with odd values of  $J+l$  have larger excitation cross sections than the ones with even values. This theoretical rule has been well confirmed by our experimental data. In addition, we have deduced theoretically that  $Q(J=0) > Q(J=2)$  for the  $np$  states, and  $Q(J=1) > Q(J=3)$  for  $nd$ ; and in a more restricted way, that  $Q(J=1) > Q(J=3)$  for  $np$  and  $Q(J=2) > Q(J=0, 4)$  for  $nd$ . These relations are in good agreement with experiment with only a few exceptions. Most of the qualitative and semiquantitative features of the experimental data can be understood from generalization of the results of helium and by simple theoretical considerations. The excitation cross sections of the states with odd values of  $J+l$  have been calculated by the Born approximation using atomic wave functions constructed by the Hartree-Fock-Slater orbitals, together with a semiempirical treatment of the intermediate vector coupling. The agreement between the theoretical and experimental values is generally satisfactory. The even- $(J+l)$  states are strongly influenced by indirect coupling; thus, no attempt was made to compare the experimental data of these states with the Born-approximation calculations.

### I. INTRODUCTION

The subject of electron excitation of atoms has received much attention in recent years. Despite its relative simplicity compared to many other collision processes, most of the published works have been largely confined to helium, hydrogen, and a few others including mercury, and some alkali and rare-gas atoms.<sup>1</sup> The studies of helium have provided us with very useful qualitative descriptions of the excitation processes from which one can understand the difference in the magnitudes of the cross sections and in the shapes of the excitation functions of the various states in terms of the Russell-Saunders coupling scheme. These qualitative descriptions were found to be applicable to

the case of mercury provided one takes into account the deviations from the Russell-Saunders coupling.<sup>2</sup> Quantitative comparisons of the experimental data with theoretical calculations, however, have not been completely successful even for the case of helium, and considerable discrepancy still exists between theory (Born approximation) and experiment in some of the cross sections.<sup>3-5</sup> It has been indicated that more refined calculations than the Born approximation are necessary in some cases.<sup>6</sup>

We have conducted a detailed study of electron excitation of the neon atoms. Other than their importance from the standpoint of lasers, the noble-gas atoms are of special interest because of the large number of states which can be studied

by the optical method and because of the breakdown of the  $LS$  coupling in these atoms. One can then test whether the general conclusions deduced from the studies of helium can be extended to the heavier atoms to explain the magnitudes of the excitation cross sections of a large number of states and their variations with incident energy in a semi-quantitative manner. The results of the neon work may also provide the foundation for studying the heavier noble gases and other atoms of the intermediate-coupling type. Because of the complexity of the atomic structure, wave functions of high accuracy for the excited states are not readily available and the calculations of the excitation cross sections are much more difficult than the calculations for helium. The results of our work also furnish an indication as to what accuracy one can expect of a Born-type calculation using wave functions constructed by the Hartree-Fock-Slater orbitals together with a semiempirical treatment of the intermediate vector coupling.

## II. EXPERIMENTAL TECHNIQUE

The excitation cross sections measured and reported herein result from observations at an angle of  $90^\circ$  relative to the electron beam. These are classified as *optical* cross sections and differ from *level* cross sections. The latter are obtained from the former by taking into consideration (a) cascade into the level from higher states, (b) the availabil-

ity of several channels for radiative decay, and (c) the anisotropic property of the radiation pattern. When the anisotropy varies with electron energy, the two classes of excitation functions vary in shape as well as in magnitude. The *apparent* excitation function of a level is obtained by adding the optical cross sections of the lines having a common upper level, i. e., taking into account only correction (b) above.

The apparatus used to measure the excitation cross sections by the optical method may be divided into four constituent components: (i) a vacuum system, (ii) an electron gun which produces a constant flux of electrons, (iii) light detection and data processing equipment, and (iv) an absolute standard source of photons with which to calibrate the detection system. The electron beam was produced by an indirectly heated barium-impregnated cathode and directed into the field-free collision region by an electron gun of pentode type. The apparatus for detecting the radiation and measuring relative excitation functions is displayed in Fig. 1. More detailed descriptions of the apparatus can be found in the papers by St. John *et al.*<sup>7</sup> and by Anderson *et al.*<sup>2</sup> The neon gas was a mass-spectrometer-controlled grade supplied by Linde Air Products Co.

A continuous scan of the spectral lines of the neon atoms in the collision chamber was made in the 3300–12000-Å region. By making relative

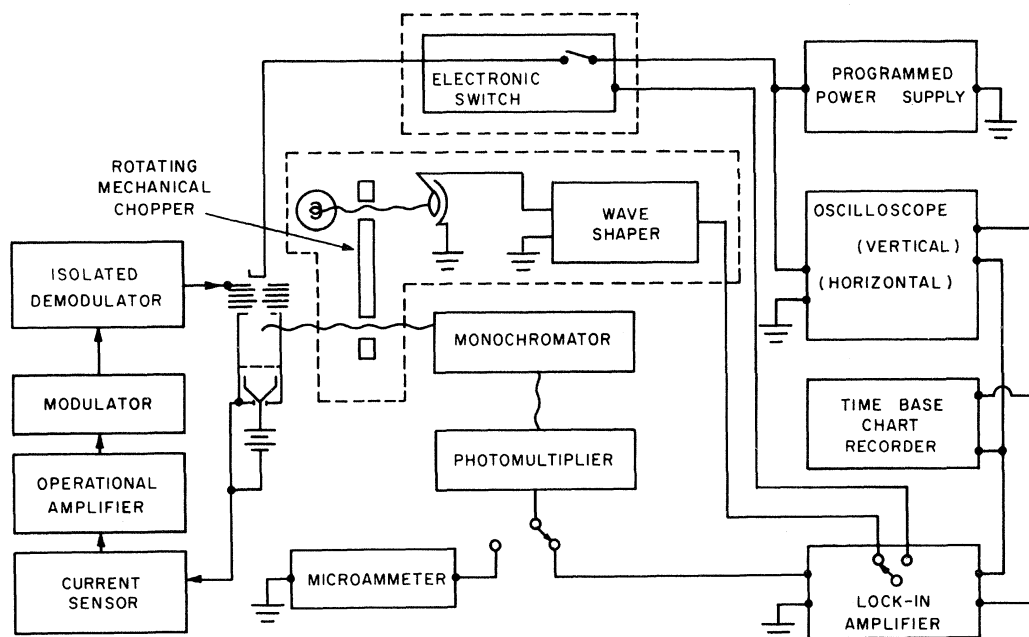


FIG. 1. Light detection and data processing system. (Light signal is modulated by either the modulator or the mechanical chopper.)

intensity measurements with a chart recorder it was possible to estimate the excitation cross sections of the very weak lines. Upper limits were placed upon the cross sections of those spectral lines in which no noticeable signal stood out above the background on the spectrogram.

The optical cross section  $Q_{jk}$  of a particular radiative transition is directly proportional to the entire photon flux  $F_{jk}$  emitted per sec by the  $j \rightarrow k$  transition from the collision chamber  $c$  as the electron beam traverses a length  $L$  of the gas. They are related as

$$F_{jk} = Q_{jk}(I/e)NL, \quad (1)$$

where  $I$  is the electron current,  $e$  is the electronic charge, and  $N$  is the gas density. The photon flux  $F_{jk}$  is determined absolutely through a calibration process<sup>8</sup> which involves the observation by the detection system of light from a tungsten-ribbon standard lamp  $s$  which has a photon radiancy  $R(\lambda, T, \Delta\lambda)$ . The quantity  $R(\lambda, T, \Delta\lambda)$  is the rate of emission of photons, in the wavelength range from  $\lambda - \Delta\lambda$  to  $\lambda + \Delta\lambda$  by the standard lamp at a true temperature  $T$ , which are transmitted by the monochromator. It depends upon Planck's blackbody formula, the emissivity of tungsten, and the transmittance of the monochromator. Also, determinations must be made of the effective radiation area  $A_s$  of the standard lamp, the solid angles of observation of the sources  $\Omega_c$  and  $\Omega_s$ , the transmittances of the parts of the beams not held in common  $\gamma_c$  and  $\gamma_s$ , and the output signals  $I_c$  and  $I_s$  of the detection system due to observation of the two sources. As shown in Eq. (5.28) of St. John's paper,<sup>8</sup> quantities relate as

$$F_{jk} = 4\pi A_s R(\lambda, T, \Delta\lambda) \frac{\Omega_s \gamma_s I_c}{\Omega_c \gamma_c I_s}. \quad (2)$$

Combination of Eqs. (1) and (2) gives

$$Q_{jk} = \frac{4\pi e}{IN} R(\lambda, T, \Delta\lambda) \frac{A_s}{L} \frac{\Omega_s \gamma_s I_c}{\Omega_c \gamma_c I_s}. \quad (3a)$$

In order to simplify the determination of the ratio  $\Omega_s/\Omega_c$ , the optical path from the standard lamp was made to simulate that from the collision chamber. This was accomplished by mounting the imaging lens, monochromator, and photomultiplier tube as a unit so it could be rotated to admit radiation from either the collision chamber or the standard lamp. Since both viewing windows were made from the same material and of the same thickness and the source-to-lens distance was the same for both modes, the arrangement was equivalent to replacing the collision chamber by the standard lamp. Hence  $\gamma_s/\gamma_c$  is equal to unity. With this particular optical arrangement the ratio  $\Omega_s/\Omega_c$  may be written in terms of the

respective diameters  $D_s$  and  $D_c$  of the aperture stop for the two modes as  $\Omega_s/\Omega_c = D_s^2/D_c^2$ . Also, since magnification of unity was adopted for our particular optical arrangement, the ratio  $A_s/L$  is simply equal to the width  $H$  of an auxiliary slit which made physical contact with the monochromator entrance slit, the long dimension of the slits being perpendicular to each other. The auxiliary slit was used when fluxes from the standard lamp were measured, and set one dimension of  $A_s$ .

In terms of experimentally measurable quantities, the cross-section equation for our system is

$$Q_{jk} = (4\pi eH/IN) R(\lambda, T, \Delta\lambda) (D_s^2/D_c^2) (I_c/I_s). \quad (3b)$$

The emissivity data reported by Devos<sup>9</sup> was used to make the non-blackbody corrections for the standard lamp. The bandpass of the monochromator which decreases slightly with increasing wavelength was determined experimentally for use in the cross-section determinations. The fluxes were modulated by the technique illustrated in Fig. 1, sensed by a photomultiplier tube, amplified, and detected by a phase-sensitive lock-in amplifier. The output signal of the lock-in amplifier from the two sources  $I_c$  and  $I_s$ , respectively, was recorded by a strip chart recorder. Care was exercised to ensure that the lock-in amplifier and chart recorder responded linearly over the range of photomultiplier signals used in the investigation.

Special precautions were taken to ensure that the light entering the monochromator always fell within the rectangular area of the grating and to make certain that none of the light exiting the monochromator overflowed the photosensitive surface area of the photomultiplier tube. For a more detailed discussion of the apparatus and its operation, see Ref. 8.

Cross sections and excitation functions were obtained from observations of the radiant flux emitted normal to the electron beam. The strong lines were emitted with little or no polarization. This was indicated by the comparison of excitation functions of the same transition made with flux having parallel and perpendicular components, respectively. No difference was noted within a pair of patterns. When polarized light is emitted from the collision chamber, its relative compositions change with electron energy, and the emission is anisotropic. A lack of polarization indicates an isotropic emission and that the ratio of the solid angle of observation to  $4\pi$  can be used in the calculation of the cross section without the aid of a correction factor.

The optical excitation cross sections of neon were measured over a range of energy from threshold to 200 eV. With the exception of the very weak

near-infrared lines ( $2s \rightarrow 2p$  and  $3d \rightarrow 2p$ ), beam currents never exceeded  $500 \mu\text{A}$  and gas pressures were kept below  $30 \text{ mTorr}$ . A detailed study of the light output as a function of beam current and gas density was carried out for the ten most prominent transitions connecting the  $2p \rightarrow 1s$  levels. The results of these experiments, illustrated in Fig. 2 for the  $2p_9$  upper level, showed that the light output always varied linearly with current and pressure for the conditions stated above.

### III. THEORY

A comprehensive theoretical treatment of the vector coupling problem in two-electron spectra, including those of atomic configurations of the type  $2p^5nl$ , has been given by Cowan and Andrew.<sup>10</sup> The Hamiltonian of the free neon atom is taken to include all the Coulomb interaction between the electrons and spin-orbit coupling of the form

$$\sum_i \xi_i (\vec{r}_i) (\vec{l}_i \cdot \vec{s}_i), \quad (4)$$

where the summation is carried out over all electrons outside of closed shells. The orbit-orbit and spin-other-orbit terms are neglected. From the one-electron orbitals  $R_{nl}(r) Y_{lm}(\theta, \phi)$ , one can construct the basis functions of the  $LS$  representation and set up the energy matrix in this representation. Within a configuration like  $2p^5nl$ , the energy matrix elements may be expressed in terms

TABLE I. Comparison of theoretical and experimental values of radiative lifetime of 19 excited states.

States	Lifetime (nsec)		States	Lifetime (nsec)	
	Theory	Expt (Ref. 15)		Theory	Expt (Ref. 14)
$1s_4$	30.5	$31.7 \pm 1.6$	$2p_1$	13.1	$14.4 \pm 0.3$
$1s_2$	2.25	$1.87 \pm 0.18$	$2p_2$	16.2	$18.8 \pm 0.3$
$2s_4$	9.50	$9.67 \pm 0.50$	$2p_3$	14.8	$17.6 \pm 0.2$
$2s_2$	10.0	$7.78 \pm 0.80$	$2p_4$	15.4	$19.1 \pm 0.3$
$3d_5$	12.5	$13.2 \pm 0.6$	$2p_5$	17.5	$19.9 \pm 0.4$
$3d_2$	8.67	$7.25 \pm 0.6$	$2p_6$	19.3	$19.7 \pm 0.2$
$3s'_1$	11.6	$12.3 \pm 0.6$	$2p_7$	17.4	$19.9 \pm 0.4$
$3s_4$	24.5	$19.5 \pm 0.5$	$2p_8$	17.8	$19.8 \pm 0.2$
$3s_2$	29.6	$23.1 \pm 1.5$	$2p_9$	17.2	$19.4 \pm 0.6$
			$2p_{10}$	23.8	$24.8 \pm 0.4$

of the Slater-Condon parameters and the spin-orbit coupling constants. These parameters are then chosen so that the solutions of the energy secular equation give the best fit to the experimental level spacings of the  $2p^5nl$  configuration. For example, in the case of  $2p^5np$ , the experimental energies of the ten levels of this configuration were used to determine three Slater-Condon parameters ( $F_2, G_0, G_2$ ) and two spin-orbit coupling constants ( $\xi_{2p}, \xi_{np}$ ).<sup>11</sup> The wave functions corresponding to the intermediate-coupling case are then expressed as linear combinations of the  $LS$ -basis functions. The radial part of the one-electron orbitals  $R_{nl}(r)$  were obtained by the Hartree-Fock-Slater self-consistent field method.<sup>12</sup> The transition probabilities between states of some ten configurations have been calculated from these wave functions and were used in analyzing the experimental data (see Sec. VI). A list of some of the values may be found in Sharpton's dissertation.<sup>8</sup> Recently, the radiative lifetimes of all the  $2p$  states and part of the  $1s, 2s, 3s, 3s'$ , and  $3d$  states have been measured.<sup>13-15</sup> A comparison of the experimental data with the theoretical values derived from these transition probabilities is illustrated in Table I. While the agreement between theory and experiment is generally satisfactory for the 19 states reported, in some other cases the uncertainty of the theoretical transition probabilities may be much higher. This happens when the product of the radial wave functions of the initial and final states  $r^3 R_{nl}(r) R_{n'l'}(r)$  is positive in some regions of  $r$  and negative in others in such a manner that its integral over  $r$  from 0 to  $\infty$  becomes very small due to cancellation. In other words the calculated transition probabilities depend sensitively on the wave functions in the overlapping region. An example is the case of  $2p^5 5p$  versus  $2p^5 3s$ . As a test of this sensitivity, we have used three sets of wave functions, i. e.,

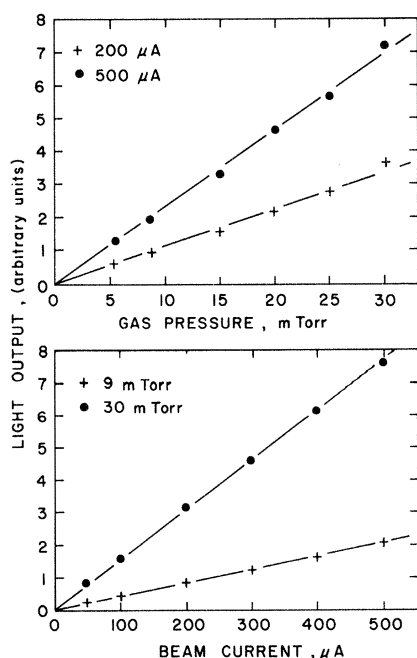


FIG. 2. Control experiments for the  $2p_9 \rightarrow 1s_2$  line at  $100 \text{ eV}$ .

the Hartree-Fock-Slater functions, the Hartree statistical-exchange scheme,<sup>16</sup> and the Coulomb approximation,<sup>17</sup> to evaluate the integral  $\int_0^\infty R_{3s}(r) \times R_{5p}(r) r^3 dr$ . The results of these three cases are 0.12, 0.12, and 0.28 a.u., respectively. Great care must be taken when using the theoretical transition probabilities to evaluate the apparent excitation cross sections from the experimental data of optical cross sections.

The electron-collision excitation cross sections can now be calculated by means of the Born approximation. Since the wave functions of the excited states are expressed as linear combinations of  $LS$ -basis functions, the excitation transition integrals can be decomposed into components corresponding to singlet-singlet and singlet-triplet transitions. The Born approximation (without exchange) was used to handle the integrals of the type  $\Delta S = 0$ , whereas the singlet-triplet integrals were evaluated by the Ochkur approximation.<sup>18</sup> Using this method, we have calculated excitation cross sections of the states associated with several configurations of the type  $2p^5ns$ ,  $2p^5np$ , and  $2p^5nd$ . Each  $2p^5ns$  configuration contains four states which are designated in the Paschen notation as  $s_2, s_3, s_4$ , and  $s_5$ , and are characterized by the total  $J$  values 1, 0, 1, and 2, respectively. Their wave functions are readily expressible in terms of the  $LS$ -basis functions  $\phi$  of the same configuration as

$$\begin{aligned} \psi(ns_2, J=1) &= \alpha\phi(^1P_1) + \beta\phi(^3P_1) , \\ \psi(ns_4, J=1) &= -\beta\phi(^1P_1) + \alpha\phi(^3P_1) , \\ \psi(ns_3, J=0) &= \phi(^3P_0) , \\ \psi(ns_5, J=2) &= \phi(^3P_2) . \end{aligned} \quad (5)$$

Of special interest is the fact that the  $s_3$  and  $s_5$  states are pure triplet within the one-configuration approximation, as mixing occurs for only  $LS$  functions of the same value of  $J$  in any intermediate-coupling scheme. Thus, excitation to these two states takes place largely through exchange between the incident and the atomic electrons; hence excitation functions have narrow peaks near the threshold analogous to the case of triplet-state excitation of helium.<sup>7</sup> Furthermore, the cross sections of the  $s_3$  and  $s_5$  are in general much smaller than those of  $s_2$  and  $s_4$ . Figure 3 shows the theoretical (Born approximation) excitation functions of the states of the  $2p^55s$  configuration. We note that the two mixed states ( $J=1$ ) have much broader excitation functions than the other two.

For the  $2p^5np$  configurations, the  $J=3$  state is a purely triplet type ( $^3D_3$ ) and hence should have excitation functions similar to those of  $ns_3$  and  $ns_5$ . However, a more detailed consideration

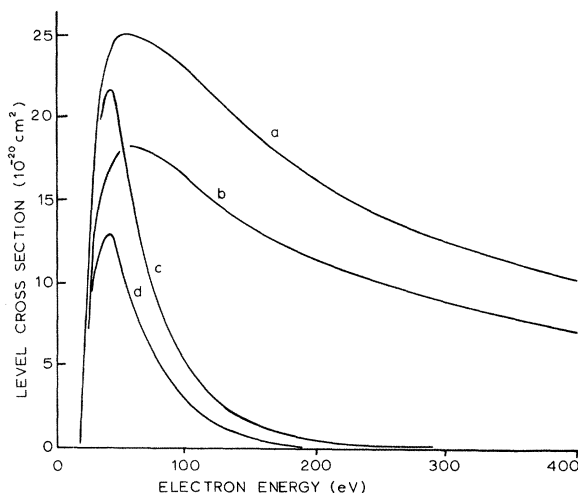


FIG. 3. Theoretical level excitation functions of the  $3s$  family calculated by the Born and Born-Ochkur approximation. Curves a, b, c, and d give  $Q(3s_4)$ ,  $Q(3s_2)$ ,  $6Q(3s_3)$ , and  $18Q(3s_5)$ , respectively.

shows that the Born cross sections of some of the mixed states also vanish when the exchange between the incident and atomic electrons is neglected. This may be seen in the following way. If we denote the atomic electrons exclusive of the  $(1s)^2(2s)^2$  core by the subscripts 1-6, and the incident electron by 7, the Coulomb interaction between the incident electron and the atomic electrons is

$$V(1, 2, \dots, 7) = \sum_{i=1}^6 (1/r_{i7}) . \quad (6)$$

For excitation from the ground state  $\psi_i (J=0, 2p^6 | 1, 2, \dots, 6)$  to an excited state  $\psi_f (J, M_J, 2p^5 3p | 1, 2, \dots, 6)$ , the interaction potential connecting these two states is

$$\begin{aligned} V_{fi}(7) &= \int \psi_f^* V \psi_i dr_1 \dots dr_6 \\ &= \sum_{i=1}^6 \int \psi_f^* \frac{1}{r_{i7}} \psi_i dr_1 \dots dr_6 . \end{aligned} \quad (7)$$

To perform the integration, we expand a typical member on the right-hand side as<sup>11</sup>

$$\frac{1}{r_{17}} = \frac{1}{r} \sum_k \sum_{q=-k}^k 4\pi \begin{pmatrix} r < \\ r > \end{pmatrix}^k \frac{Y_{kq}^*(\theta_7 \phi_7) Y_{kq}(\theta_1 \phi_1)}{2k+1} . \quad (8)$$

To the extent that configuration interactions are neglected, the atomic wave functions  $\psi_i$  and  $\psi_f$  consist of linear combinations of products of one-electron orbitals of the type  $R_{2p}(r) Y_{1m}(\theta, \phi)$  and  $R_{3p}(r) Y_{1m}(\theta, \phi)$ . When the integration over the coordinates of each electron is carried out for Eq. (7), only the terms of  $k=0$  and  $k=2$  in the expansion of Eq. (8) survive. On the other hand, since  $\psi_i, \psi_j$ , and  $Y_{kq}(\theta_1 \phi_1)$  are eigenfunctions of  $J$  cor-

responding to eigenvalues of  $0, J$ , and  $k$ , respectively, the integral

$$\int \psi_f^* r^{-1} (r_</r_>)^k Y_{kq}(\theta_1, \phi_1) \psi_i dr_1 \cdots dr_6 \quad (9)$$

vanishes unless  $J=k$ . Thus,  $V_{fi}$  becomes zero for the  $J=1$  and  $J=3$  states of  $2p^5np$ , leading to zero cross sections under the nonexchange Born approximation. Theoretical excitation functions of selected members of  $2p^53p$  calculated by the Born-Ochkur approximation are displayed in Fig. 4. We note that the states with odd  $J$  exhibit narrow maxima in the curves.

Although the Coulomb potential gives no direct excitation interaction of the ground state with the  $2p^53p$ ,  $J=1$ , and  $J=3$  states, indirect coupling via the  $J=0$  and  $J=2$  states of the same configuration may occur and broaden the excitation functions of the states with odd  $J$  over those shown in Fig. 4. The importance of the indirect coupling in the excitation of the  $3^1D$  state of helium has been recently demonstrated.<sup>6</sup> A detailed calculation of cross sections due to indirect coupling, however, is beyond the scope of this paper. Furthermore, configuration interactions may also provide Coulomb coupling with the ground state. Nevertheless, for electron energy considerably larger than the threshold, one may expect that the cross sections of the odd- $J$  states are smaller than those of the even- $J$  states, i. e.,

$$Q(2p^5np, J=0, 2) > Q(2p^5n^t, J=1, 3) \quad (10)$$

Among the states which interact directly with the

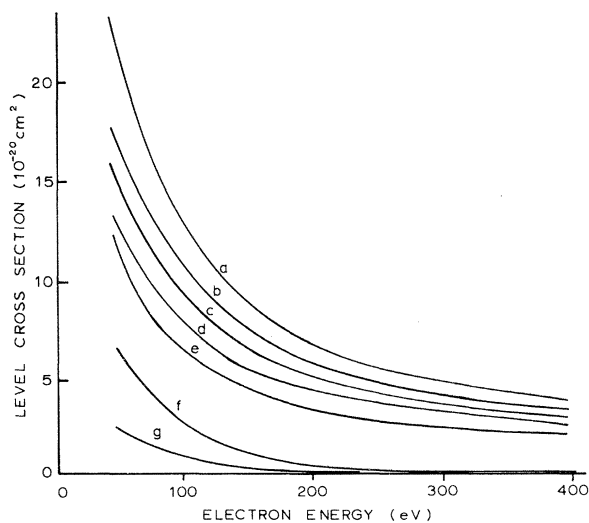


FIG. 4. Theoretical level excitation functions of seven  $2p$  levels calculated by the Born and Born-Ochkur approximation. Curves a, b, c, d, e, f, and g give  $0.04 Q(2p_1)$ ,  $\frac{1}{4}Q(2p_6)$ ,  $Q(2p_8)$ ,  $Q(2p_4)$ ,  $Q(2p_3)$ ,  $Q(2p_5)$ , and  $Q(2p_7)$ , respectively.

ground state, one can further expect

$$Q(2p^5np, J=0) > Q(2p^5np, J=2) \quad (11)$$

because the former involves integrals similar to (9) with  $k=0$  which are generally larger than the ones with  $k=2$  that are responsible for exciting the  $J=2$  states. The distinction between the indirect-coupling excitation cross sections of the  $J=1$  and of the  $J=3$  states is less apparent. However, we note that the  $2p^53p$ ,  $J=3$  state is a pure triplet  $^3D_3$ . If we assume that the relative strength between the ground state  $i$  and the  $^3D_3$  state  $f$  via each of the intermediate states  $k$  of the configuration  $2p^5np$  is proportional to  $V_{fk} V_{ki}$ , and that the effect due to each intermediate state of this group is additive, then the sum of  $V_{fk} V_{ki}$  over all the intermediate states of the same configuration vanishes when the states  $i$  and  $f$  have different total spin. The assumptions cited above are, of course, very approximate in nature. However, this does suggest the possibility of a strong cancellation of the indirect-coupling effect due to the various intermediate states so that the net indirect coupling for the purely triplet state is much less significant than that for the  $J=1$  states. This leads to the conclusion that as a rule the purely triplet states have cross sections smaller than the odd- $J$  states with mixed spin multiplicity, or

$$Q(2p^5np, J=1) > Q(2p^5np, J=3) \quad (12)$$

For the same reason the  $J=3$  states are expected to have narrower excitation functions than the  $J=1$  states. Since (12) was obtained with the aid of approximations which may be rather crude, it should not be taken to be of the same degree of validity as (10) and (11). In deriving all three inequalities (10)–(12), it was implicitly assumed that all the “mixed” states have a substantial component of the singlet  $LS$  eigenfunction. If this singlet component accidentally becomes very small for a particular mixed state, the cross section of this state may decrease to the extent that (10)–(12) are no longer satisfied. In Sec. VI, we see that such exceptions do occur for the  $2p^53p$  configuration.

For the  $2p^5nd$  configurations, the interaction integrals vanish for  $J=0, 2$ , and  $4$ . The  $J=0$  and  $J=4$  states are purely triplet ( $^3P_0$  and  $^3F_4$ ), whereas the states with  $J=2$  are of the singlet-triplet mixed type. Based on the theoretical consideration given above, one obtains

$$Q(2p^5nd, J=1, 3) > Q(2p^5nd, J=0, 2, 4) \quad (13)$$

$$Q(2p^5nd, J=1) > Q(2p^5nd, J=3) \quad (14)$$

$$Q(2p^5nd, J=2) > Q(2p^5nd, J=0, 4) \quad (15)$$

corresponding to (10), (11), and (12), respectively.

Again, (13) and (14) have a more general validity than (15). Also, one anticipates the narrowest peaks in the excitation functions of the two purely triplet states. Excitation functions have been calculated for all the  $2p^5 4d$  states using the Born and Born-Ochkur approximation. The theoretical cross sections will be given along with the experimental results in Sec. VI.

One can apply the same kind of group-theoretical analysis to the  $2p^3 ns$  configuration as well, and obtain indeed the same results as those stated in the latter part of the paragraph where Eqs. (5) appear. The rule of classification of the magnitude of the excitation cross sections according to whether  $J$  is even or odd for all  $ns$ ,  $np$ , and  $nd$  states as derived from group-theoretical arguments, e. g., (10) and (13), can be summarized as follows: *Within a given configuration  $2p^5 nl$ , the states with odd values of  $J+l$  generally have larger excitation cross sections than do the ones with even  $J+l$  at electron energies considerably above the threshold.* Among each group of states of either even or odd  $J+l$ , the variation of the cross section with respect to  $J$  may be described by (11), (12), (14), and (15). Experimental tests of these rules are discussed in Sec. VI.

Veldre, Lyash, and Rabik<sup>19,20</sup> calculated excitation cross sections of neon by the Born approximation. These authors used hydrogenic wave functions and considered  $LS$ ,  $jl$ , and  $jj$  coupling; thus, no attempts were made to compare our calculated cross sections with theirs.

#### IV. EXPERIMENTAL RESULTS

The identification of spectral lines with the appropriate transitions for neon were extensively studied by Paschen.<sup>21</sup> To avoid confusion between the configuration notation and Paschen's notation, we shall write  $2p^5 nl$  for a singly excited configuration, whereas, the symbols  $ns$ ,  $np$ , and  $nd$ , which are not prefaced by  $2p^5$ , refer to Paschen's designation. In this work, we have studied optical excitation functions of the transitions  $ns \rightarrow n'p$ ,  $np \rightarrow n's$ , and  $nd \rightarrow n'p$ . The experimental data are presented in this section and are followed by a discussion of the general shape of the excitation functions in Sec. V. Cascade analysis, evaluation of level excitation cross sections, and comparison of the results with theory will be presented in Sec. VI.

##### A. $2p$ Family

The excitation functions displayed in Fig. 5 illustrate how the optical cross sections of the ten  $2p$  levels of neon vary from onset to 200 eV. The curves were obtained by measuring the radiant flux emitted from spectral lines which were well

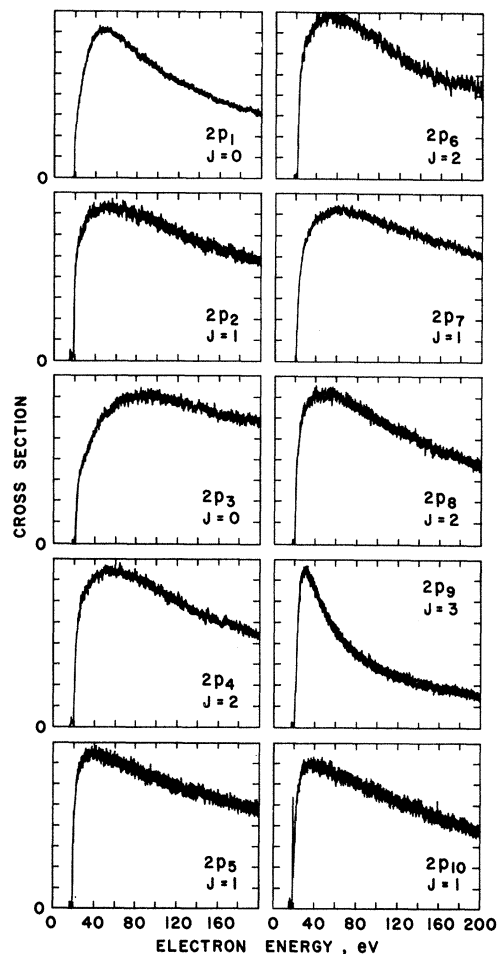


FIG. 5. Optical excitation functions of the  $2p$  family.

isolated from any known neighboring line of significant intensity with the bandpass of the monochromator set at  $6 \text{ \AA}$  or less. The absolute cross sections of 30 transitions originating from the  $2p$  levels were experimentally measured at an electron energy of 100 eV. The results are presented in Table II. The low-energy part of the  $2p_{10}$  function is shown in Fig. 6. The spike occurring at 18.6 eV is attributed to resonance and will be discussed in Sec. V B.

The limits placed upon the experimental errors were based solely upon the experimental repeatability, i. e., independent cross-section determinations at different times, for various beam currents and gas pressures within the range previously specified, and for different temperatures of the standard lamp. An error analysis was made of the measuring devices, e. g., the electron beam current meter, the lock-in amplifier, the chart recorder, the McLeod gauge, and the standard-lamp current monitor. Consideration was even

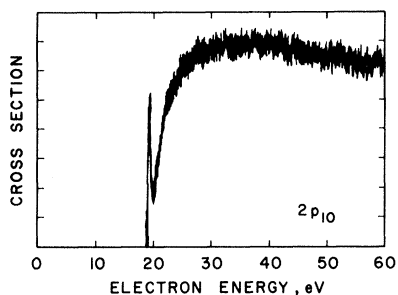


FIG. 6. Optical excitation function of the  $2p_{10}$  level showing the spike.

given to the scattering of the standard lamp within the monochromator for some regions of the spectrum. Only the uncertainties in the standard-lamp ribbon, e.g., the emissivity of tungsten and the calibration of the true temperature, were excluded in the consideration of factors which were believed would introduce errors into the cross-section measurements. This analysis resulted in an estimate of the probable experimental error of 5–10%, an amount less than the uncertainty of the cross sections yielded by the experimental measurements. The sources of the uncertainties of the cross sections lie in instrument noise and instability as well as in the accuracy of the measurement devices. The noise and instabilities are considered random in nature and dominate in causing the uncertainties. Each cross section listed in our table is the arithmetic mean value, and the uncertainty is the standard deviation of the cross sections obtained for the transition.

Up to this time, very little experimental excitation data has existed for neon. The most extensive contributions have been made by Hanle<sup>22</sup> and by Herrmann.<sup>23</sup> Hanle's results consist of 16 relative excitation functions for spectral lines of the  $2p \rightarrow 1s$  series over an energy range from threshold to 100 eV. No absolute intensity measurements were reported in his paper. Herrmann, on the other hand,

published no excitation functions of neon. His work consisted of measurements of the maxima of the absolute optical cross section of 14 spectral lines belonging to the  $2p \rightarrow 1s$  series and three lines cascading into the  $2p_5$  and  $2p_9$  levels. Table III contains a comparison of our maximum cross sections with those of Herrmann. The relative shapes presented by Hanle and the absolute data published by Herrmann appear to agree quite well with our data when one considers that the early data were obtained through the use of photographic plates in contrast to photomultiplier tubes of modern experiments. In a more recent paper by Zapesochnyi and Feltsan,<sup>24</sup> the excitation functions of three prominent spectral lines belonging to the  $2p \rightarrow 1s$  series are presented. The general features of the three curves resemble the excitation functions of the  $2p_1$ ,  $2p_4$ , and  $2p_9$  levels displayed in Fig. 5. The locations of the peaks are the same in both works. However, the excitation functions reported here fall off more rapidly with electron energy than do those of Zapesochnyi and Feltsan.

#### B. $3p$ Family

In order to see how the optical excitation functions change as the  $n$  value is increased, the  $3p$  family of functions was obtained for comparison with the  $2p$  family. Great care had to be exercised in order to obtain the ten desired excitation functions of this family, as the  $3p$  levels are more closely spaced than are the corresponding  $2p$  levels; hence greater resolution was required from the monochromator. Furthermore, the presence of Ne II lines causes additional complications. It was necessary that slit widths of about 0.1 mm be used for some cases; only the  $3p \rightarrow 1s$  transitions which were resolved from neighboring Ne II spectral lines were studied. Most of the  $3p$  curves retain the general shape of their  $2p$  counterpart. Only those showing significant change are displayed in Fig. 7. The reasons for the differences in shape are explained in Sec. V.

TABLE II. Optical cross sections  $Q_{jk}$  of the spectral lines for the series  $2p \rightarrow 1s$  at 100 eV in units of  $10^{-20} \text{ cm}^2$ .

$k \setminus j$	$2p_1$	$2p_2$	$2p_3$	$2p_4$	$2p_5$	$2p_6$	$2p_7$	$2p_8$	$2p_9$	$2p_{10}$
$1s_2$	$168 \pm 13$	$18 \pm 3^a$	0.20 $\pm 0.05$	$43 \pm 6^a$	$19 \pm 2^a$	$35 \pm 4$	$1.9 \pm 0.6$	$6.2 \pm 0.7$	...	$0.9 \pm 0.2$
$1s_3$	...	$9.8 \pm 2.1^a$	...	...	$19 \pm 3$	...	$11 \pm 2$	...	...	$3.2 \pm 0.5$
$1s_4$	$1.9 \pm 0.2$	$4.1 \pm 0.6$	$37 \pm 6$	$33 \pm 5$	$0.8 \pm 0.1$	$7.8 \pm 1.5$	$35 \pm 7$	$53 \pm 8$	...	$13 \pm 2$
$1s_5$	...	$8.9 \pm 1.4$	...	$19 \pm 3$	$3.4 \pm 0.6^a$	$53 \pm 9^a$	$7.0 \pm 1.5$	$29 \pm 4^a$	$32 \pm 3^a$	$33 \pm 3$
$\sum_{1s} Q_{jk}$	$170 \pm 13$	$41 \pm 7$	$37 \pm 6$	$95 \pm 14$	$42 \pm 6$	$96 \pm 15$	$55 \pm 11$	$88 \pm 13$	$32 \pm 3$	$50 \pm 6$

<sup>a</sup>Spectral line corresponding to this transition could not be completely resolved from an adjacent less intense one. Adjustments were made by employing theoretical branching ratios.

TABLE III. Comparison of different experimental data of the peak optical cross sections (in units of  $10^{-20}$  cm<sup>2</sup>) of some  $2p-1s$  lines.

Wavelength (Å)	Transition	$Q_{jk}$ (max)	
		This work	Herrmann
5852	$2p_1-1s_2$	225 ± 15	172
5945	$2p_4-1s_5$	21 ± 3	19
6074	$2p_3-1s_4$	38 ± 6	29
6096	$2p_4-1s_4$	37 ± 4	30
6143	$2p_6-1s_5$	63 ± 9	69
6217	$2p_7-1s_5$	7.5 ± 1.3	12
6266	$2p_5-1s_3$	22 ± 4	27
6334	$2p_8-1s_5$	34 ± 5	38
6383	$2p_7-1s_4$	38 ± 6	39
6402	$2p_9-1s_5$	91 ± 16	90
6507	$2p_8-1s_4$	64 ± 10	65
6678	$2p_4-1s_2$	48 ± 7	72

In Table IV, the absolute values of the optical cross sections of the ten  $3p$  curves are given for an electron energy of 100 eV. These values were used in obtaining the apparent cross sections of the  $3p$  levels as well as estimates of cascade from the ten  $3p$  into the four  $2s$  levels.

#### C. $ns$ Families

Each  $ns$  family is composed of four energy levels ( $ns_2, ns_3, ns_4,$  and  $ns_5$ ). Due to an inadequate level of detectivity for the spectral region of the  $2s-2p$  lines (9000–17 000 Å), it was impossible to obtain optical excitation functions for the family. However, curves were plotted for the  $3s,$   $4s,$  and  $5s$  families. The optical excitation functions of lines originating from the levels of these three families have the following interesting features: (i) The curves do not show any noticeable variation in shape with  $n$  value; because of this fact, only the excitation functions of the  $3s$  family are presented in Fig. 8; (ii) the shape of the  $ns_2$

TABLE IV. Absolute optical cross sections (in units of  $10^{-20}$  cm<sup>2</sup>) of the prominent spectral lines belonging to the  $3p-1s$  series.

Wavelength (Å)	Transition	$Q_{jk}$ at 100 eV
3520	$3p_1-1s_2$	12 ± 2
3461	$3p_2-1s_3$	0.4 ± 0.1
3454	$3p_3-1s_4$	2.8 ± 0.6
3594	$3p_4-1s_2$	1.3 <sup>a</sup>
3467	$3p_5-1s_3$	0.7 ± 0.2
3448	$3p_6-1s_5$	1.5 ± 0.4
3501	$3p_7-1s_4$	1.1 ± 0.2
3464	$3p_8-1s_5$	1.2 ± 0.2
3473	$3p_9-1s_5$	1.2 ± 0.3
3511	$3p_{10}-1s_5$	1.4 ± 0.4

<sup>a</sup> $Q_{jk}$  value which was measured represents the sum of the transitions  $3p_4-1s_2$  and  $3p_2-1s_2$ . The contribution of the latter was estimated from the cross section of the  $3p_2-1s_3$  transition together with the theoretical transition probabilities, and was subtracted from the sum of  $Q_{jk}$  of the two unresolved lines.

and  $ns_4$  excitation functions are almost identical and to a slightly less extent the same may be said of the  $ns_3$  and  $ns_5$  excitation functions; (iii) finally, the curves show no resemblance to the excitation functions of the  $np$  levels which cascade into them. Table V gives the optical cross sections of all significant  $j \rightarrow k$  transitions connecting the  $ns$  families with the  $2p$  family.

#### D. $nd$ Families

Each  $nd$  family is composed of 12 energy levels. These are designated in the Paschen notation by the symbols  $nd'_1, nd''_1, nd''_2, nd_3, nd_4, nd'_4, nd_5, nd_6, ns'_1, ns''_1, ns'''_1,$  and  $ns''''_1$ . Selected optical excitation functions of this family are given in Fig. 9. Since the  $d$  levels are so closely spaced, only four ( $d_2, d_3, d_4,$  and  $s'_1$ ) of the 12 types of levels yielded lines completely resolved from other lines.

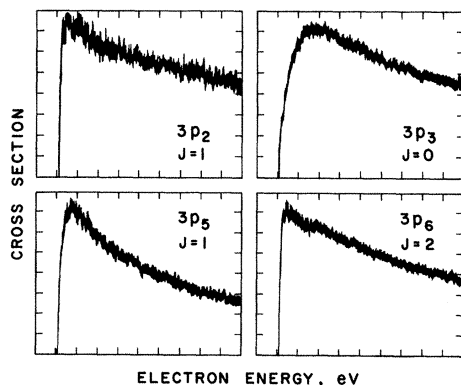


FIG. 7. Optical excitation functions belonging to the  $3p$  family.

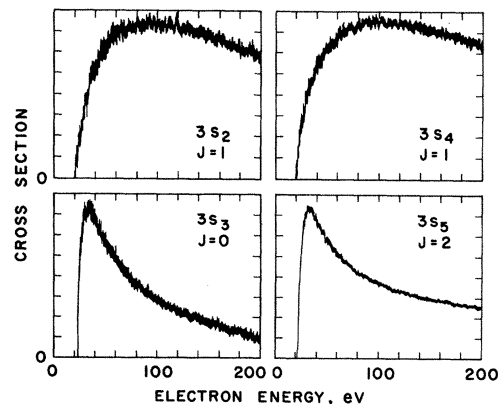


FIG. 8. Optical excitation functions of the  $3s$  family.

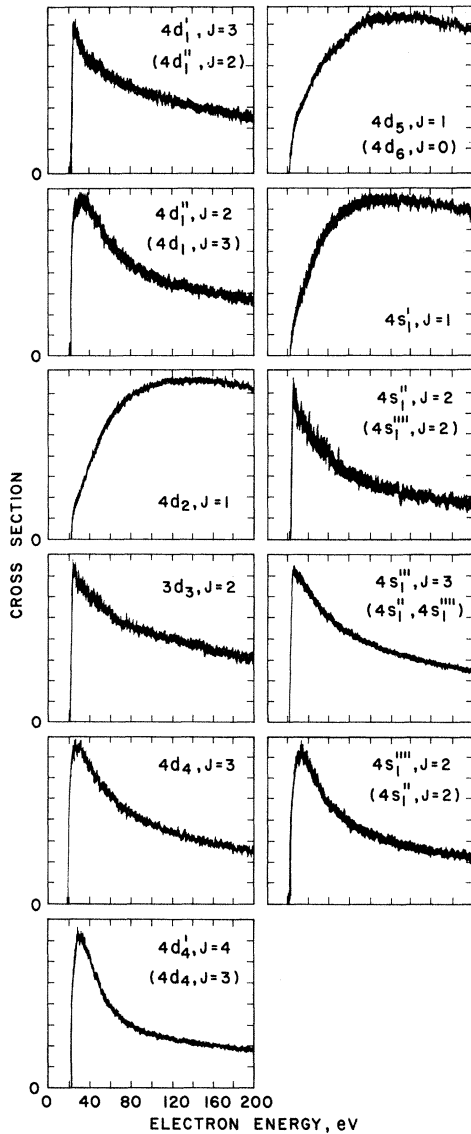


FIG. 9. Optical excitation functions of the  $d$  levels. When two or more states are indicated, those in parentheses contribute an insignificant amount of intensity and do not influence the shape of the excitation function.

In several of the other cases, the state being studied produced at least one line considerably stronger in intensity than the neighboring lines, judged from a comparison of transition probabilities. The dominant line controlled the shape of the composite excitation function and hence yielded the shape of the excitation function of the level under consideration. The  $d_6$  state failed to produce dominating lines of sufficient intensity for measurements of excitation functions. The states listed in Fig. 9 which are enclosed in parentheses are considered to be of secondary importance in controlling the

excitation function with which the listing is associated.

Table VI gives the optical cross sections of all significant  $j \rightarrow k$  transitions connecting the  $nd$  families with the  $2p$  family. Since many of the  $nd$  levels merge as the  $n$  value is increased, resolution of the spectral lines presented a real problem. As one goes to higher  $n$  values, the  $ns_1'$ ,  $ns_1''$ ,  $ns_1'''$ , and  $ns_1''''$  levels shift closer to each other while at the same time the  $nd_1'$ ,  $nd_1''$ ,  $\dots$ ,  $nd_6$  levels also shift closer to each other. Thus, the radiation into the  $2p$  levels coming from the  $d$  levels is reported in the last two rows of Table VI for  $n$  values of 5, 6, and 7 as though it originated from two distinct levels. (The merging of levels for increasing  $n$  values also occurs for the  $ns$  families, i. e.,  $ns_2$  and  $ns_3$  merge while at the same time  $ns_4$  and  $ns_5$  merge.) The cross sections of those transitions originating at levels greater than  $9s$  or  $7d$  were found to be less than  $10^{-22}$  cm<sup>2</sup> at 100 eV. This represents the detectivity limit of the system employed in this investigation.

#### V. GENERAL FEATURES OF EXCITATION FUNCTIONS

We present here a discussion of the general qualitative features of the excitation functions. We shall point out a few analogies between neon and helium; hence, we shall first summarize the essential results of helium<sup>7</sup>:

(a) Those levels having optically allowed transitions connecting with the ground state, i. e., the  $^1P$  levels, possess a very broad excitation function whose maximum occurs around 100 eV. The  $^1S$  and  $^1D$  levels have considerably narrower excitation functions with maximum values located near 50 eV. The excitation functions of the  $^3S$ ,  $^3P$ , and  $^3D$  levels are characterized by a very sharp peak around 30 eV, which declines very rapidly at higher energy.

(b) The cross sections of the singlet levels are in general much larger than those of the triplet levels having the same  $n$  value. Furthermore, among the singlet levels the cross sections of the optically allowed  $^1P$  states are much larger than those of the  $^1S$  and  $^1D$  states having the same  $n$  value.

#### A. $ns$ Families

The states capable of dipole-allowed transitions to the ground state are of the type  $2p^5ns$ ,  $J=1$ , or  $ns_2$  and  $ns_4$  in Paschen's notation. Figure 8 shows that these states indeed have the broadest excitation functions. The excitation functions of  $ns_3$  and  $ns_5$  are seen to exhibit narrow peaks. As explained in Sec. III,  $ns_3$  and  $ns_5$  are purely triplet states and thus have excitation functions similar to those of triplet states of helium. Further-

TABLE V. Optical cross sections<sup>a</sup>  $Q_{jk}$  of the spectral lines for the series  $ns-2p$  at 100 eV in units of  $10^{-20}$  cm<sup>2</sup>.

$k \setminus j$	$2p_1$	$2p_2$	$2p_3$	$2p_4$	$2p_5$	$2p_6$	$2p_7$	$2p_8$	$2p_9$	$2p_{10}$
$2s_2$	1.1 <sup>b</sup>	5.5 <sup>b</sup>	1.1 <sup>b</sup>	9.2 <sup>b</sup>	3.2 <sup>b</sup>	9.7	1.3 ± 0.5	0.9 <sup>b</sup>	...	2.3 <sup>b</sup>
$2s_3$	...	< 0.8 <sup>b</sup>	...	...	< 1.0 <sup>b</sup>	...	< 1.5 <sup>c</sup>	...	...	< 0.6 <sup>b</sup>
$2s_4$	0.4 <sup>b</sup>	< 0.1 <sup>b</sup>	2.1 <sup>b</sup>	1.1 <sup>b</sup>	3.2 <sup>b</sup>	5.0 <sup>b</sup>	5.9 <sup>b</sup>	20	...	4.2
$2s_5$	...	0.4 <sup>b</sup>	...	1.3 <sup>b</sup>	0.2 <sup>b</sup>	1.1 <sup>b</sup>	0.2 <sup>b</sup>	1.4 <sup>b</sup>	6.7 <sup>b</sup>	2.7 ± 0.8
$3s_2$	0.5	3.3 <sup>b</sup>	0.8	3.2 <sup>b</sup>	1.3	0.8	0.5	0.4	...	0.4
$3s_3$	...	0.3	...	...	1.8	...	0.3	...	...	< 0.1
$3s_4$	1.0	0.1 <sup>b</sup>	1.1 ± 0.5	0.3 <sup>b</sup>	2.7 <sup>b</sup>	3.2	3.0 <sup>b</sup>	7.4 ± 2.0	...	1.0
$3s_5$	...	0.12	...	0.7 <sup>b</sup>	< 0.1	0.7 ± 0.2	0.2	0.6	2.5	0.8
		± 0.04								
$4s_2$	0.1 <sup>b</sup>	0.4	0.1	1.1	0.2	0.3	< 0.1	0.1	...	0.2
$4s_3$	...	< 0.1 <sup>b</sup>	...	...	0.1	...	< 0.1	...	...	< 0.1
$4s_4$	0.2 <sup>b</sup>	< 0.1	0.2	< 0.1 <sup>b</sup>	0.3	0.9	0.8	1.6	...	0.3
$4s_5$	...	< 0.1	...	< 0.1	< 0.1	0.2	< 0.1	0.1	0.6	0.2
$\sum_{j=5,6,7,8,9} Q_{jk}$	0.1	0.1	0.1	0.7	0.2	0.7	0.4	0.8	0.3	0.1

<sup>a</sup>Errors approximately 20% unless otherwise specified.<sup>c</sup>Estimated from experimental data.<sup>b</sup>Estimated using theoretical branching ratios.

more, from the results of helium as well as theoretical considerations, we expect the cross sections for the  $ns_2$  and  $ns_4$  states to be larger than those of  $ns_3$  and  $ns_5$ . This is shown to be the case in Sec. VIC.

The curves shown in Fig. 8 are proportional to the apparent excitation functions. In order to obtain level excitation functions and to compare them with theory, the cascade contributions must be

subtracted from the total population of the excited states. The major cascade transitions to the  $ns$  states ( $n > 1$ ) lie in the long-wavelength region to which our detection apparatus is rather insensitive. Although it is possible to ascertain the cascade contribution by using theoretical transition probabilities (see Sec. VI), some of the transition probabilities are subject to a very high degree of uncertainty, making it difficult to ob-

TABLE VI. Optical cross sections<sup>a</sup>  $Q_{jk}$  of the spectral lines for the series  $nd-2p$  at 100 eV in units of  $10^{-20}$  cm<sup>2</sup>.

$k \setminus j$	$2p_1$	$2p_2$	$2p_3$	$2p_4$	$2p_5$	$2p_6$	$2p_7$	$2p_8$	$2p_9$	$2p_{10}$
$3s'_1$	2.5	{4.4}	5.0 <sup>b</sup>	0.1 <sup>b</sup>	0.6 <sup>b</sup>	0.2 <sup>b</sup>	{2.0}	0.2 <sup>b</sup>	...	1.2
$3s''_1$	...	...	...	< 0.1 <sup>b</sup>	< 0.1 <sup>b</sup>	0.2 <sup>b</sup>	< 0.1 <sup>b</sup>	< 0.1 <sup>b</sup>	~ 0 <sup>b</sup>	0.5
$3s'''_1$	...	...	...	{3.7}	...	1.1 <sup>b</sup>	...	0.7 ± 0.3	< 0.1 <sup>b</sup>	...
$3s''''_1$	...	~ 0 <sup>b</sup>	...	...	1.2	< 0.1 <sup>b</sup>	1.3 <sup>b</sup>	< 0.1 <sup>b</sup>	< 0.1 <sup>b</sup>	~ 0 <sup>b</sup>
$3d'_1$	...	...	...	0.8 <sup>b</sup>	...	2.2 <sup>b</sup>	...	...	...	...
$3d''_1$	...	~ 0 <sup>b</sup>	...	< 0.1 <sup>b</sup>	0.4	< 0.1 <sup>b</sup>	0.6 <sup>b</sup>	{0.9}	{1.5}	~ 0 <sup>b</sup>
$3d_2$	4.7 <sup>b</sup>	< 0.1 <sup>b</sup>	4.6 <sup>b</sup>	1.5	5.1	< 0.1 <sup>b</sup>	7.8 <sup>b</sup>	2.2	...	2.9
$3d_3$	...	< 0.1 <sup>b</sup>	...	...	< 0.1 <sup>b</sup>	2.2 ± 0.6	< 0.1 <sup>b</sup>	< 0.1 <sup>b</sup>	0.2 <sup>b</sup>	1.8
$3d_4$	...	...	...	{4.3}	...	0.9 <sup>b</sup>	...	4.2	...	...
$3d'_4$	...	...	...	...	...	...	...	...	{3.4}	...
$3d_5$	0.3 <sup>b</sup>	{1.3}	1.1	0.7 <sup>b</sup>	~ 0 <sup>b</sup>	1.3	< 0.1 <sup>b</sup>	0.3 <sup>b</sup>	...	7.9
$3d_6$	...	...	...	...	< 0.1 <sup>b</sup>	...	< 0.1 <sup>b</sup>	...	...	1.0 ± 0.3
$4s'_1$	0.7	1.5	2.2	< 0.1	0.4	< 0.1	0.4	< 0.1	...	0.4
$4s''_1$	...	...	...	...	...	...	...	...	...	...
$4s'''_1$	...	0.8	...	1.7	0.6	0.1	0.2	0.2	~ 0 <sup>b</sup>	0.2
$4s''''_1$	...	...	...	...	...	...	...	...	...	...
$4d'_1, 4d''_1$	...	~ 0 <sup>b</sup>	...	0.2	0.4 <sup>b</sup>	0.4 <sup>b</sup>	0.5	0.4	0.3	~ 0 <sup>b</sup>
$4d_2$	0.8	< 0.1	2.1	0.3 <sup>b</sup>	2.0	1.1 ± 0.6	3.3	0.9	...	0.4
$4d_3$	...	< 0.1	...	0.20 ± 0.05	< 0.1	0.3	< 0.1	< 0.1	< 0.1	0.5
$4d_4, 4d'_4$	...	...	...	< 0.1	...	0.4	...	1.6	1.1	...
$4d_5, 4d_6$	0.2 <sup>b</sup>	0.8 <sup>b</sup>	0.3 <sup>b</sup>	0.4 <sup>b</sup>	0.1	0.5	< 0.1	0.20 ± 0.05	...	2.2
(5, 6, 7)I <sup>c</sup>	0.4	0.7	0.5	0.9	0.3	0.2	0.3	0.1	< 0.1	0.5
(5, 6, 7)II <sup>d</sup>	0.2	0.2	0.7	0.1	0.5	1.4	1.4	1.7	0.8	1.1

<sup>a</sup>Errors approximately 20% unless otherwise specified.<sup>b</sup>Estimated using theoretical branching ratios.<sup>c</sup>This group includes the  $ns'_1$ ,  $ns''_1$ ,  $ns'''_1$ , and  $ns''''_1$ states with  $n = 5, 6, 7$ .<sup>d</sup>This group includes the  $nd'_1$ ,  $nd''_1$ ,  $nd_2$ ,  $nd_3$ ,  $nd'_4$ ,  $nd_5$ , and  $nd_6$  states with  $n = 5, 6, 7$ .

tain reliable cascade estimates. Nevertheless, if it is assumed that the excitation cross sections of the optically allowed states of the  $2p^5ns$  are larger than those of the  $2p^5np$  states of the same  $n$ , it is expected that cascade from high  $2p^5n'p$  states to the optically allowed states contributes but a small fraction of the population of those states. This is further supported by the observation that all the  $ns_2$  and  $ns_4$  states have excitation functions of the same shape which differs greatly from the excitation curves of any of the  $np$  states. If cascading were to contribute a significant part of the population of the  $ns_2$  or  $ns_4$  state, the shape of their excitation functions would be distorted by those of the  $n'p$  states and the degree of distortion would vary for different  $n$ . The constancy of the shape of these functions with different  $n$  values suggests a negligible cascade component. In the absence of a detailed cascade analysis, we shall therefore assume that the graphs for  $ns_2$  and  $ns_4$  in Fig. 8 are representative of the level excitation functions. The same kind of reasoning cannot be applied to the  $ns_3$  and  $ns_5$  states since their direct excitation cross sections could be smaller than those of some of the higher  $n'p$  states. If the apparent excitation cross sections of  $ns_3$  and  $ns_5$  do include appreciable cascade, the direct excitation functions of the  $ns_3$  and  $ns_5$  should be even narrower than those shown in Fig. 8. Indeed, the slight difference in the curves of  $3s_3$  and  $3s_5$  may be ascribed to the larger cascade population of the latter state (see Sec. VIC).

The shape of the experimental excitation functions of the  $ns_2$  and  $ns_4$  is in good qualitative agreement with the theoretical curves. The discrepancy in the energy corresponding to maximum cross section between theory (65 eV) and experiment (90 eV) is to be expected in view of the use of the Born approximation. One recalls a similar situation for the  $n^1P$  states of helium in which the peak excitation occurs at 100 eV in contrast to the Born theoretical value of 60 eV.<sup>7</sup> Measurements of the excitation functions of selected  $ns_2$  and  $ns_4$  states have been extended to 350 eV. From 200 to 350 eV, the rate of decrease of the excitation cross sections with energy agrees well with the Born-approximation calculations.

#### B. $2p$ and $3p$ Families

Of the ten states arising from the  $2p^53p$  configuration, only the  $2p_9$  state is a purely triplet state ( $^3D_3$ ). Inspection of the  $2p_9$  function in Fig. 5 reveals an optical excitation function with a sharp peak around 30 eV and a fast-declining tail at higher energy. All the other optical excitation functions of the  $2p$  family possess moderately broad peaks. This is in accordance with the the-

oretical discussion given in Sec. III. It should be noted that even though the excitation functions of these nine levels are broad, none are as broad as the  $ns_2$  and  $ns_4$  levels which have optically allowed transitions to the ground state. This feature again is analogous to the case of helium.

The auxiliary sharp peak at 18.6 eV observed in the optical excitation function of the  $2p_{10}$  state may be ascribed to resonance associated with a negative-ion state. The same resonance peak has been observed before<sup>25,26</sup> in the study of electron scattering and metastable excitation cross sections. The only other  $2p$  states which lie below 18.6 eV are  $2p_9$  and  $2p_8$  (18.55 and 18.57 eV), but the radiation from the resonance level was too weak to be detected by the equipment used in these experiments in the excitation functions of  $2p_9$  and  $2p_8$ . A careful study of resonance peaks in the  $2p$  states is being conducted by Walker and St. John.<sup>27</sup>

In the  $3p$  family, the  $3p_9$  state exhibits a triplet-type sharp excitation similar to that of  $2p_9$ . Also the optical excitation functions of  $3p_1$ ,  $3p_4$ ,  $3p_7$ ,  $3p_8$ , and  $3p_{10}$  are very similar to the corresponding  $2p$  states except the  $3p_{10}$  function exhibits no spike. The  $3p$  curves showing significant change in shape over their  $2p$  counterpart are those shown in Fig. 7. These curves have sharper peaks shifted toward lower energy and their tails decline faster with increasing energy than do their  $2p$  counterparts. This can be explained on the basis that the  $2p$  states receive more cascade from the higher levels than  $3p$  states, resulting in larger distortion of the level excitation functions. Of these four sets of optical excitation functions, the  $p_3$  set illustrates this concept most significantly. Each  $p_3$  level is fed by five levels ( $s'_1$ ,  $s_2$ ,  $s_4$ ,  $d_2$ , and  $d_5$ ), each of which has a broad excitation function with a maximum near 100 eV. Subtraction of the cascade contributions of the  $2s_2$ ,  $2s_4$ ,  $3s'_1$ ,  $3d_2$ , and  $3d_5$  levels from the optical excitation function of the  $2p_3$  state will yield a curve having a shape similar to the optical excitation function of the  $3p_3$  level.

A quantitative analysis of the cascade is presented in Sec. VI, where the level excitation functions of the  $2p$  states are evaluated and compared with the Born theoretical values.

Finally, we come to the consideration of whether or not the cross sections of the optically allowed members of the  $2p^5ns$  group are larger than those of the  $2p^5np$  states. In Sec. VIC we indicate that for the  $2p^54s$  group, ( $2s$  in Paschen's notations) the apparent cross sections of  $2s_2$  and  $2s_4$  are  $11 \times 10^{-19}$  and  $13 \times 10^{-19}$  cm<sup>2</sup>, respectively, at 100 eV but no attempt was made to correct for cascade. These values may be taken as a good ap-

proximation to the level cross section in view of the relatively small cascade population of the  $ns_2$  and  $ns_4$  states as explained previously. This may be compared with the value of  $6.4 \times 10^{-19} \text{ cm}^2$  for the  $3p_1$  state which is the largest cross section of the  $2p^5 4p$  group (see Sec. VIB). A similar comparison may be made between  $2p^5 5s$  and  $2p^5 5p$ . The cross sections of  $3s_2$  and  $3s_4$ , as will be shown in Sec. VIC, are  $6.0 \times 10^{-19}$  and  $10 \times 10^{-19} \text{ cm}^2$ , respectively, at 100 eV, whereas, the comparable cross section for the  $4p_1$  state of the  $2p^5 5p$  configuration is  $1.7 \times 10^{-19} \text{ cm}^2$ , and cross sections of all other  $4p$  members are considerably smaller. Thus, it is seen that the optically allowed states of the  $2p^5 ns$  group do indeed have higher cross sections than the  $2p^5 np$  members of the same  $n$ .

### C. $nd$ Families

For a given  $nd$  family, two of the 12 levels are pure triplet states, and are designated as  $nd'_4$  ( $^3F_4$ ) and  $nd_6$  ( $^3P_0$ ). The exact shape of the excitation function of any  $nd'_4$  level could not be obtained free of contaminating radiation from the  $nd_4$  level. Furthermore, the only transition from an  $nd_6$  level ( $3d_6-2p_{10}$ ) which could be obtained free of  $nd_5$  radiation was so weak that we were unable to make reliable measurements of the excitation function. Nevertheless, from Fig. 9 we see that the excitation function of the combination of the  $4d'_4-2p_9$  and  $4d_4-2p_9$  transitions falls off considerably more rapidly than that of  $4d_4-2p_8$  alone; hence, it is in accordance with the observation that the triplet states have sharp excitation functions. In addition, all three optically allowed states ( $ns'_1$ ,  $nd_2$ , and  $nd_5$ ) were found to have very broad peaks in their excitation functions as shown in Fig. 9. The remaining states exhibit excitation curves of intermediate breadth.

From the results of the evaluation of the level cross sections which will be presented in Sec. VID, we have the cross sections at 100 eV of the three optically allowed states  $4s'_1$ ,  $4d_2$ , and  $4d_5$ , as  $2.1 \times 10^{-19}$ ,  $6.1 \times 10^{-19}$ , and  $1.3 \times 10^{-19} \text{ cm}^2$ , respectively, as compared to the corresponding value of  $6.4 \times 10^{-19} \text{ cm}^2$  for  $3p_1$ . Hence, for the  $2p^5 nd$  configuration, the optically allowed states do not have cross sections as large as the ones in  $2p^5 ns$ ; instead, their cross sections are similar in magnitude to those of the  $2p^5 np$ ,  $J=0$  states.

### VI. DETERMINATIONS OF APPARENT AND LEVEL EXCITATION CROSS SECTIONS

For the  $2p$  levels the intensities of the transitions to all the lower states were measured. We obtained the apparent excitation cross sections by summing the experimentally measured optical cross sections  $Q_{jk}$  over all the lower states  $k$ ,

without having to use theoretical transition probabilities, and thus eliminated one major source of uncertainty. For all the other states, it was necessary to employ the theoretical transition probabilities to determine the apparent excitation cross sections from the optical data. Subtracting the cascade contributions of all higher levels from the apparent excitation cross section yielded the level (direct) excitation cross section  $Q_j$  of the  $j$ th state, since the radiation was very nearly isotropic.

### A. $2p$ Family

The apparent excitation cross sections at 100 eV of all ten  $2p$  levels were obtained by adding the appropriate entries in Table II. The excitation functions displayed in Fig. 5 were then used to determine the apparent cross sections from onset to 200 eV. Cascade corrections were made by using the data presented in Tables V and VI and Figs. 8 and 9. Cascade contributions to the  $2p$  levels from levels above  $9s$  and  $7d$ , estimated to be less than 3%, were neglected. The level excitation cross sections of the  $2p$  states are given in Table VII for electron energies ranging from 18 to 200 eV.

The experimental data in Table VII do confirm the theoretical prediction of larger cross sections for states with odd  $J+l$  (see Sec. III), i. e.,  $Q(J=0, 2) > Q(J=1, 3)$  for the  $2p$  group, with the exception of  $2p_3$ . Another theoretical deduction  $Q(J=0) > Q(J=2)$  as given in (10) is seen to be true of  $2p_1$ , but  $2p_3$  has cross sections smaller than those of the  $J=2$  states. The reason for this becomes apparent if we inspect the wave functions of the  $2p_1$  and  $2p_3$  states which can be expressed as linear combinations of the basis functions in the  $LS$  coupling as

$$\begin{aligned} \psi(2p_1) &= \alpha \phi(2p^5 3p, ^1S_0) + \beta \phi(2p^5 3p, ^3P_0) , \\ \psi(2p_3) &= \beta \phi(2p^5 3p, ^1S_0) - \alpha \phi(2p^5 3p, ^3P_0) . \end{aligned} \quad (16)$$

Using the intermediate-coupling scheme of calculation as outlined in the first part of Sec. III, we found  $\alpha = 0.99$  and  $\beta = 0.14$ . Since  $\phi(2p^5 3p, ^1S_0)$  is the major contributor to the cross sections, the unusually low value of  $\beta$  is responsible for the "anomalously" small cross section of  $2p_3$ . At 100 eV, all the  $J=1$  and  $J=3$  states have about the same cross section, but as the energy is increased to 200 eV, the cross section of the pure triplet state  $2p_9$  does indeed drop below those of the  $J=1$  states as predicted by (12) with the exception of  $2p_{10}$ . Upon examining the data in Table VII, we observe that while all four  $J=1$  states have apparent excitation functions of about the same width, the level excitation function of  $2p_{10}$

TABLE VII. Level cross sections<sup>a</sup> of the  $2p$  states in units of  $10^{-20}$  cm<sup>2</sup>.

State	$J$	Energy (eV)															
		22	24	28	30	32	36	40	50	60	80	100	120	140	160	180	200
$2p_1$	0	86	113	153	172	181	202	214	218	210	181	157	136	121	106	96	90
$2p_2$	1	18	20	25	27	28	28	29	28	27	25	23	21	19	17	16	15
$2p_3$	0	9	12	14	15	15	16	17	18	17	17	15	14	13	12	11	11
$2p_4$	2	44	48	55	59	61	65	68	73	73	70	64	57	50	47	43	40
$2p_5$	1	24	28	27	27	27	26	25	24	22	19	16	14	13	12	12	12
$2p_6$	2	40	49	63	66	69	73	75	78	76	69	61	52	45	40	38	36
$2p_7$	1	23	25	28	29	29	31	31	31	30	28	24	22	20	18	16	14
$2p_8$	2	46	51	56	56	58	59	60	59	57	49	41	35	29	24	20	17
$2p_9$	3	36	51	53	53	51	48	44	37	31	22	18	13	12	10	8	6
$2p_{10}$	1	26	29	33	33	33	33	32	29	26	21	17	13	10	8	6	5

<sup>a</sup>With the exception of  $2p_{10}$  for which a resonance peak at 18.6 eV was observed, the level cross sections below 22 eV can be obtained by interpolation with the value of zero at the onset. For  $2p_{10}$  the level cross sections at 18.6 and 20 eV are 46 and  $18 \times 10^{-20}$  cm<sup>2</sup>, respectively.

falls off more rapidly than those of the others. In fact, the shapes of the level excitation functions of  $2p_{10}$  and  $2p_9$  are rather alike except for the sharp resonance spike (18.6 eV) present only in the former, suggesting that the excitation of  $2p_{10}$  is less influenced by indirect coupling (see Sec. III) than the other three states of the same  $J$ . The explanation for this "anomalous" property of the  $2p_{10}$  state lies again on the specific form of the wave function. In general the wave function for any one of the  $J=1$  states may be written as a linear combination of the  $LS$  eigenfunctions of  $^1P_1$ ,  $^3S_1$ ,  $^3P_1$ , and  $^3D_1$ . Our intermediate-coupling calculations (Sec. III) give the coefficients of the  $^1P_1$  member in the wave functions of the  $2p_2$ ,  $2p_5$ ,  $2p_7$ , and  $2p_{10}$  states as 0.57, 0.78, 0.25, and 0.08, respectively. In other words, of these four states,  $2p_{10}$  has by far the smallest singlet component, which is mainly responsible for the indirect coupling, and therefore should behave more like the purely triplet state  $2p_9$  as far as excitation cross sections are concerned.

Comparison between the experimental and theoretical cross sections at 100 and 200 eV is shown in Table VIII. Since the Born approximation was used for the theoretical calculations, meaningful comparison can be made only for the  $J=0$  and  $J=2$  states, as the indirect coupling which is neglected in the calculation is mainly responsible for the cross sections of the other states. In addition to the inherent uncertainty of the Born approximation and the uncertainty of the Hartree-Fock-Slater radial wave function, the intermediate-coupling coefficients introduce another source of inaccuracy. As explained in Sec. III these coupling coefficients were obtained by fitting the experimental energy level spacings within a configuration to a simplified theoretical model rather than by a completely first-principle calculation. In view of the approximations adopted in the cal-

culations, the agreement between theory and experiment at 200 eV is considered as satisfactory except for the  $2p_4$  states. More accurate wave functions of the excited states are needed before making a critical test of the Born approximation.

#### B. $3p$ and $4p$ Families

For the  $3p$  family, it was necessary to resort to theoretical branching ratios in order to determine the apparent excitation cross sections. The results are therefore subject to the uncertainty of the theoretical transition probabilities. A second kind of uncertainty arises when estimates of cascade into the  $3p$  states are made. Since the  $ns \rightarrow 3p$  and  $nd \rightarrow 3p$  cascade transitions lie beyond the spectral detectivity region of our system, cascade estimates had to be inferred from ex-

TABLE VIII. Experimental values of apparent and level cross sections of the  $2p$  states at 100 and 200 eV and comparison with the theoretical level cross sections in units of  $10^{-20}$  cm<sup>2</sup>.

States	$J$	100 eV			200 eV		
		Expt. app. Q	Expt. level Q	Theoret. level Q	Expt. app. Q	Expt. level Q	Theoret. level Q
$2p_1$	0	170	160	330	103	90	180
$2p_3$	0	37	15	7.0	31	11	3.6
$2p_4$	2	95	64	8.0	63	40	4.4
$2p_6$	2	96	61	45	64	36	24
$2p_8$	2	87	41	10	55	17	5.5
$2p_2$	1	41	23	0.15 <sup>a</sup>	30	15	0.020 <sup>a</sup>
$2p_5$	1	42	16	0.12 <sup>a</sup>	32	12	0.014 <sup>a</sup>
$2p_7$	1	55	24	1.2 <sup>a</sup>	42	14	0.23 <sup>a</sup>
$2p_{10}$	1	50	17	14 <sup>a</sup>	33	5	2.0 <sup>a</sup>
$2p_9$	3	35	18	3.0 <sup>a</sup>	18	6	0.60 <sup>a</sup>

<sup>a</sup>Since allowance of indirect coupling was not made in the Born-Ochkur approximation, little physical significance can be attached to the theoretical cross sections of the odd- $J$  states given in this table. These numbers are included merely to provide some measures of the magnitude of cross sections which one can expect of the effect of electron exchange alone.

perimental data on transitions from a particular upper state to a  $2p$  level along with the theoretical transition probabilities from this upper state to the  $2p$  and  $3p$  states. For the analysis of the  $3p$  states, we have taken into account cascades from only  $3s$ ,  $4s$ , and  $4d$ . The level cross sections were taken as the difference between the apparent cross section and the cascade estimate, both subject to a sizable uncertainty. When these two quantities become nearly the same, as in the cases of  $3p_5$ ,  $3p_7$ ,  $3p_9$ , and  $3p_{10}$  at 200 eV, the level cross sections determined by this method have little quantitative significance. In Table IX, we present the experimental values of the apparent and level cross sections along with the theoretical level cross sections at 100 and 200 eV for the  $3p$  states. The experimental level cross sections here are of distinctly lower accuracy than the ones for  $2p$ . It is difficult to make an estimate of the errors as the major source of uncertainty originates from the use of theoretical transition probabilities, the accuracy of which is not known. In the absence of such an estimate, we have chosen somewhat arbitrarily to give the apparent cross sections in two significant figures although this is not to be taken as an index of the accuracy of the experimental data. The level cross sections, however, may involve much larger errors, and are in most cases given to only one significant figure. The even- $J$  states clearly have larger cross sections than those with odd  $J$ . In addition,  $Q (J=0) > Q (J=2)$  is evident. Unlike the  $2p$  counterparts, the level cross sections of  $3p_3$  are larger than those of the  $J=2$  states. Examination of our intermediate-coupling calculations shows that for the  $3p$  the coefficients  $\alpha$  and  $\beta$  as defined similar to Eqs. (16) are 0.88 and 0.47, respectively. With much less disparity between  $\alpha$  and  $\beta$ , the

TABLE IX. Experimental values of apparent and level cross sections of the  $3p$  states at 100 and 200 eV and comparison with the theoretical level cross sections in units of  $10^{-20}$  cm<sup>2</sup>.

States	$J$	100 eV			200 eV		
		Expt. <sup>a</sup> app. Q	Expt. <sup>a</sup> level Q	Theoret. level Q	Expt. <sup>a</sup> app. Q	Expt. <sup>a</sup> level Q	Theoret. level Q
$3p_1$	0	66	64	80	42	41	43
$3p_3$	0	13	10	23	9.1	7	12
$3p_4$	2	7.9	5	7.0	5.6	4	3.8
$3p_6$	2	8.9	4	5.0	6.0	2	2.7
$3p_8$	2	12	3	6.9	8.2	1	3.6
$3p_2$	1	4.6	1	0.55 <sup>b</sup>	3.6	1	0.073 <sup>b</sup>
$3p_5$	1	3.3	1	0.30 <sup>b</sup>	1.9	...	0.060 <sup>b</sup>
$3p_7$	1	8.2	1	0.13 <sup>b</sup>	6.0	...	0.026 <sup>b</sup>
$3p_{10}$	1	5.4	1	4.5 <sup>b</sup>	4.3	...	0.60 <sup>b</sup>
$3p_3$	3	4.3	1	1.0 <sup>b</sup>	2.2	...	0.21 <sup>b</sup>

<sup>a</sup>For discussions of the accuracy of the experimental values, see Sec. VIB and Sec. VII, paragraph (i).

<sup>b</sup>See Footnote a of Table VIII.

“anomaly” of having a smaller cross section for a  $J=0$  state than the  $J=2$  states which happens for the  $2p$  family, now disappears. The uncertainties of the  $J=1$  and  $J=3$  cross sections are too large to make a sensible comparison of their magnitude. The agreement between theory and experiment in Table IX is quite satisfactory for the  $J=0$  and  $J=2$  states.

Efforts were made to determine the cross sections of the  $4p$  states. The  $4p-1s$  transitions are in the spectrum region around 3600 Å, where absolute standardization by means of the tungsten lamp becomes rather difficult. Furthermore, we were able to estimate cascade contributions from only the  $4s$  states. Nevertheless, we obtained for 100 eV the cross sections of the  $4p_1$ ,  $4p_3$ ,  $4p_4$ ,  $4p_6$ ,  $4p_7$ , and  $4p_8$  as  $2 \times 10^{-19}$ ,  $5 \times 10^{-20}$ ,  $3 \times 10^{-20}$ ,  $1 \times 10^{-20}$ ,  $1 \times 10^{-20}$ , and  $1 \times 10^{-20}$  cm<sup>2</sup>, respectively, whereas the cross sections of the remaining four states were estimated to be less than  $0.5 \times 10^{-20}$  cm<sup>2</sup>. These cross sections have even lower accuracy than those of the  $3p$  states, and are given here primarily to illustrate how the cross sections decrease with increasing  $n$ . We also observe that within the  $4p$  group, the states with  $J=0$  ( $4p_1$  and  $4p_3$ ) have the largest cross section, and that the states with  $J=2$  have cross sections larger than the odd- $J$  states with the exception of  $4p_7$ . The Born theoretical excitation cross sections at 100 eV for the  $4p_1$ ,  $4p_3$ ,  $4p_4$ ,  $4p_6$ , and  $4p_8$  states are, respectively,  $2.5 \times 10^{-19}$ ,  $19 \times 10^{-20}$ ,  $2.9 \times 10^{-20}$ ,  $1.8 \times 10^{-20}$ , and  $3.4 \times 10^{-20}$  cm<sup>2</sup>, which compare satisfactorily with our experimental estimates.

### C. $3s$ and $2s$ Families

The optical cross sections of the majority of the  $3s-2p$  transitions were experimentally determined (Table V). Theory was employed to fill in the missing members. In order to obtain the apparent cross sections, it was necessary that theoretical transition probabilities be used to determine the radiation from the  $3s$  to  $3p$  and to the ground state. For cascade analysis, it is first necessary to measure the  $np-1s$  transitions and deduce the  $np-3s$  intensities by employing theoretical branching ratios. By adopting this procedure we were able to obtain an estimate of the cascade from the  $4p$  into the  $3s$  states. Excitation cross sections of the  $3s$  states, both experimental and theoretical, are given in Table X. The remarks about the accuracy of the level cross sections of the  $3p$  states apply to this case.

The results in Table X reinforce our belief that the  $ns_2$  and  $ns_4$  levels receive only a small part of their population from cascade. We note that the cascade contribution to the  $3s_5$  state is much higher than that to  $3s_3$ . This is reflected in the

TABLE X. Experimental values of apparent and level cross sections of the  $3s$  states at 100 and 200 eV and comparison with the theoretical level cross sections in units of  $10^{-19}$  cm<sup>2</sup>.

States	$J$	100 eV			200 eV		
		Expt. <sup>a</sup> app. $Q$	Expt. <sup>a</sup> level $Q$	Theoret. level $Q$	Expt. <sup>a</sup> app. $Q$	Expt. <sup>a</sup> level $Q$	Theoret. level $Q$
$3s_2$	1	7.1	6.0	1.6	5.6	4.8	1.2
$3s_4$	1	11	10	2.2	9.7	9.3	1.6
$3s_3$	0	0.30	0.25	0.015	0.10	0.07	0.0023
$3s_5$	2	0.94	0.5	0.078	0.62	0.3	0.012

<sup>a</sup>For discussions of the accuracy of the experimental values, see Secs. VI B and VII, part (i).

shape of the apparent excitation functions (Fig. 8) in that the  $3s_3$  state has a narrower peak than  $3s_5$ .

The agreement between the theoretical and experimental cross section is only marginal for the optically allowed states  $3s_2$  and  $3s_4$ . The large difference between the experimental cross sections of  $3s_3$  and  $3s_5$  and the theoretical ones is not surprising because the latter, entirely due to exchange effects, are very small. Errors in the evaluation of the apparent cross section and in the cascade analysis as well as any higher-order effects in the theory which lead to Coulomb coupling of the  $3s_3$  and  $3s_5$  states with the ground state may explain this discrepancy.

Because of the lower sensitivity of our apparatus for optical detection in the infrared region where the  $2s \rightarrow 2p$  transitions lie, no measurements of the shape of the excitation functions could be made for the  $2s$  family. The only useful data which we produced were the optical cross sections of the  $2s \rightarrow 2p$  transitions at 100 eV. With the aid of theoretical transition probabilities, one finds the apparent excitation cross sections of the  $2s_2$ ,  $2s_4$ ,  $2s_3$ , and  $2s_5$  to be  $11 \times 10^{-19}$ ,  $13 \times 10^{-19}$ ,  $0.4 \times 10^{-19}$ , and  $1.4 \times 10^{-19}$  cm<sup>2</sup>, respectively, at 100 eV. No attempt was made to correct for cascade. The corresponding Born theoretical values for  $2s_2$  and  $2s_4$  are  $5.0 \times 10^{-19}$  and  $6.3 \times 10^{-19}$  cm<sup>2</sup>, respectively.

#### D. $nd$ Families

The apparent excitation functions of the  $4d$  states were obtained from measurements of the  $4d \rightarrow 2p$  transitions and the necessary theoretical branching ratios. Cascade from the  $4p$  states was estimated from the intensities of the  $4p \rightarrow 1s$  transitions along with the appropriate theoretical transition probabilities, and was found to constitute only a small part of the total population of the  $4d$  states. No measurements were made to obtain cascade corrections from the higher  $np$  states and from the  $nf$  states. In Table XI are given the experimental and theoretical cross

sections of the  $4d$  states. The experimental data again confirm the dependence of the magnitude of the cross sections on  $J+l$  as stated in (13). Furthermore, we see  $Q(J=1) > Q(J=3) > Q(J=2) > Q(J=0)$ . Particularly striking is the difference in the cross sections of the dipole-allowed states over those of the forbidden ones. The  $4d'_4(J=4)$  state, however, has a cross section nearly the same as those of the  $J=2$  states, in contrast to (15). The reasons for this discrepancy are not clear and further examinations should be interesting. It is sensible to compare the Born-approximation calculation with the experimental values only for the  $J=1$  and  $J=3$  states. The agreement here is slightly worse than for the  $2p$  and  $3p$  families.

Excitation measurements have also been made for the  $3d$  families. Since the  $3d \rightarrow 2p$  transitions are in the infrared region, it was necessary to use much higher electron beam current to detect these radiations. The efficiency of the monochromator varies quite drastically with the wavelength in the region of the  $3d \rightarrow 2p$  lines. Thus the absolute intensity measurements of these lines are less reliable than those of the  $4d \rightarrow 2p$  lines. Although the results obtained for the  $3d$  cross sections also exhibit the general ordering of  $Q(J=1) > Q(J=3) > Q(J=2) > Q(J=0)$ , we do not consider the data to be sufficiently reliable to be included in Table XI.

#### VII. DISCUSSION AND SUMMARY

(i) Electron excitation cross sections have been determined for the  $2s$ ,  $3s$ ,  $2p$ ,  $3p$ ,  $4p$ , and  $4d$  states. The major source of uncertainty in the determination of the apparent excitation cross sections is the use of theoretical transition probabilities (ex-

TABLE XI. Experimental values of apparent and level cross sections of the  $4d$  states at 100 and 200 eV and comparison with the theoretical level cross sections in units of  $10^{-20}$  cm<sup>2</sup>.

States	$J$	100 eV			200 eV		
		Expt. <sup>a</sup> app. $Q$	Expt. <sup>a</sup> level $Q$	Theoret. level $Q$	Expt. <sup>a</sup> app. $Q$	Expt. <sup>a</sup> level $Q$	Theoret. level $Q$
$4s'_1$	1	22	21	16	21	20	12
$4d_2$	1	65	61	27	64	60	21
$4d_5$	1	15	13	8.2	14	12	6.2
$4s''_1$	3	3.1	3.1	0.66	2.0	2.0	0.34
$4d'_1$	3	2.2	2.1	0.23	1.4	1.4	0.12
$4d_4$	3	3.5	3.4	1.1	2.3	2.2	0.56
$4s''_2$	2	1.6	1.6	0.042 <sup>b</sup>	1.0	1.0	0.0053 <sup>b</sup>
$4s''''_1$	2	1.3	1.3	0.023 <sup>b</sup>	0.9	0.9	0.0030 <sup>b</sup>
$4d''_1$	2	1.7	1.6	0.0074 <sup>b</sup>	1.2	1.2	0.0010 <sup>b</sup>
$4d_3$	2	1.8	1.2	0.053 <sup>b</sup>	1.3	0.8	0.0072 <sup>b</sup>
$4d_6$	0	0.6	0.3	0.020 <sup>b</sup>	0.4	0.2	0.0023 <sup>b</sup>
$4d'_4$	4	2.0	1.9	0.053 <sup>b</sup>	1.4	1.4	0.0073 <sup>b</sup>

<sup>a</sup>For discussions of the accuracy of the experimental values, see Sec. VII, part (i).

<sup>b</sup>See footnote a of Table VIII.

cept for the case of  $2p$  for which no theoretical transition probabilities need be used). Cascade generally has only minor effects on the  $ns$  and  $nd$  states, but constitutes a much larger portion of the population of the  $2p$  and  $3p$  states, typically 50%. Theoretical transition probabilities again have to be used to determine the cascade into the various states (except the  $2p$  states). Since the errors of the theoretical transition probabilities are not known, we have chosen somewhat arbitrarily to give the apparent excitation cross sections in two significant figures, even though their accuracy may vary greatly from one case to another. For some of the  $3p$  states, the cascade amounts to over 70% of the population, and consequently the level excitation cross sections are influenced more strongly by the uncertainty of the theoretical transition probabilities than are the apparent excitation cross sections. For these states, we gave only one significant figure for the level excitation cross sections.

(ii) For helium it has been found that the dipole-allowed states ( $^1P$ ) have the largest excitation cross sections and the broadest excitation functions, the triplet states have small excitation cross sections and narrow excitation functions, and the excitation behaviors of the dipole-forbidden singlet states ( $^1S$  and  $^1D$ ) are intermediate between these two extremes. Our results show that this scheme of characterization of the excitation behaviors by the quantum numbers  $L$  and  $S$  of the states can be carried over to neon provided one expresses the wave functions of the excited states in terms of the  $LS$  eigenfunctions. For example, all the dipole-allowed states of the  $2p^5ns$  and  $2p^5nd$  configurations reported here exhibit very broad excitation functions and the purely triplet states ( $2p^5ns, J=0$  and  $2; 2p^5np, J=3; 2p^5nd, J=0$  and  $4$ ) have narrow excitation functions. The wave functions of the other states can be expressed as linear combinations of wave functions of dipole-forbidden singlet states and of triplet states, thus the excitation functions of these states have intermediate widths. One minor modification to our generalization is that while the dipole-allowed states of the  $2p^5ns$  configurations indeed have the largest excitation cross sections, the observed values of the cross sections of the dipole-allowed members of the  $2p^5nd$  configurations are not all distinctly larger than those of the  $2p^5np$  states.

(iii) By primarily using a group-theoretical

argument, we have shown that within a configuration  $2p^5nl$ , the states with odd values of  $J+l$  show larger excitation cross sections than do the ones with even values. This rule has been well verified by our experimental results. For the odd- $(J+l)$  states, it can be shown theoretically that  $Q(J=0) > Q(J=2)$  for an  $np$  group, and  $Q(J=1) > Q(J=3)$  for  $nd$ . Good agreements are found with experiments. With the use of certain special assumptions, one can further deduce from theory that among the states with even values of  $J+l$ , the cross sections of the purely triplet states are smaller than those of states with mixed singlet-triplet multiplicity, e.g., (12) and (15). Most of our measured cross sections are in accordance with this theoretical deduction although a few exceptions have been noted.

(iv) For the excitation cross sections of the states with odd  $J+l$ , the agreement between experiment and Born-approximation calculations is regarded, on a whole, to be satisfactory, in view of the approximate nature of the wave functions. The even- $(J+l)$  states are strongly influenced by indirect coupling; hence, no attempt was made to compare the experimental data of these states with the Born theory.

(v) The most serious limitation of the present status of the optical method for determining excitation cross sections lies on its use of theoretical transition probabilities. This objection can be removed if one can measure all the emission lines originating from the excited states in question. Nevertheless, within the present limitations, we have studied the excitation behaviors of some 60 states. It is particularly encouraging to see that most of the qualitative and semiquantitative features can be understood from generalization of the results of helium and by simple theoretical considerations. More accurate wave functions of the excited states are especially desirable to calculate transition probabilities as well as to furnish a more critical comparison of the Born approximation with experimental data.

#### ACKNOWLEDGMENTS

The intermediate-coupling calculations of the wave functions were based on the program of Dr. R. D. Cowan, to whom we wish to express our appreciation. Thanks are also due to Kenneth G. Handy for his assistance in the analysis of the data.

\* Research sponsored in part by the Air Force Office of Scientific Research, Office of Aerospace Research, U.S. Air Force, under Grant Nos. AF-AFOSR-252-67 and AFOSR-69-1670.

<sup>1</sup>See, for example, B. L. Moiseiwitsch and S. J. Smith, *Rev. Mod. Phys.* **40**, 238 (1968).

<sup>2</sup>R. J. Anderson, E. T. P. Lee, and C. C. Lin, *Phys. Rev.* **157**, 31 (1967).

- <sup>3</sup>K. L. Bell, D. J. Kennedy, and A. E. Kingston, Proc. Phys. Soc. (London) **B2**, 26 (1969); **B1**, 204 (1968).
- <sup>4</sup>H. R. Moustafa Moussa, F. J. de Heer, and J. Schutten, Physica **40**, 517 (1969).
- <sup>5</sup>J. W. McConkey and J. M. Woolsey, in *Abstracts of Papers, Sixth International Conference on the Physics of Electronic and Atomic Collisions, Cambridge, Mass., U.S.A., 1969* (MIT Press, Cambridge, Mass., 1969), p. 355.
- <sup>6</sup>S. Chung and C. C. Lin, in Ref. 5, p. 363.
- <sup>7</sup>R. M. St. John, F. L. Miller, and C. C. Lin, Phys. Rev. **134**, A888 (1964).
- <sup>8</sup>R. M. St. John, *Methods of Experimental Physics* (Academic, New York, 1969), Vol. 8, p. 27; F. A. Sharpton, Ph.D. thesis, University of Oklahoma, 1968 (unpublished).
- <sup>9</sup>J. C. Devos, Physica **20**, 715 (1954).
- <sup>10</sup>R. D. Cowan and K. L. Andrew, J. Opt. Soc. Am. **55**, 502 (1965).
- <sup>11</sup>See, for example, E. U. Condon and G. H. Shortley, *The Theory of Atomic Spectra* (Cambridge U.P., London, 1964).
- <sup>12</sup>F. Herman and S. Skillman, *Atomic Structure Calculations* (Prentice-Hall, Englewood Cliffs, N.J., 1963).
- <sup>13</sup>J. Z. Klose, Phys. Rev. **141**, 181 (1966).
- <sup>14</sup>W. R. Bennett and P. J. Kindlemann, Phys. Rev. **149**, 38 (1966).
- <sup>15</sup>G. M. Lawrence and H. S. Liszt, Phys. Rev. **178**, 122 (1969).
- <sup>16</sup>R. D. Cowan, Phys. Rev. **163**, 54 (1967).
- <sup>17</sup>D. R. Bates and A. Damgaard, Phil. Trans. Roy. Soc. **A242**, 101 (1949).
- <sup>18</sup>V. I. Ochkur, Zh. Eksperim. i Teor. Fiz. **45**, 734 (1963) [Soviet Phys. JETP **18**, 503 (1964)].
- <sup>19</sup>V. Ya. Veldre, A. V. Lyash, and L. L. Rabik, Opt. i Spektroskopiya **19**, 319 (1965) [Opt. Spectry. USSR **19**, 182 (1965)].
- <sup>20</sup>See p. 265 of Ref. 1.
- <sup>21</sup>See, for example, C. E. Moore, Natl. Bur. Std. (U.S.) Circ. No. **467** 76 (1949), and the references therein.
- <sup>22</sup>W. Hanle, Z. Physik **65**, 512 (1930).
- <sup>23</sup>O. Herrmann, Ann. Physik **25**, 143 (1936).
- <sup>24</sup>I. P. Zapesochnyi and P. V. Feltsan, Bull. Acad. Sci. USSR Phys. Ser. **27**, 1015 (1963).
- <sup>25</sup>C. E. Kuyatt, J. A. Simpson, and S. R. Mielczarek, Phys. Rev. **138**, A385 (1965).
- <sup>26</sup>F. M. J. Pichanick and J. A. Simpson, Phys. Rev. **168**, 64 (1968).
- <sup>27</sup>K. G. Walker and R. M. St. John, Bull. Am. Phys. Soc. **15**, 421 (1970).

## Absolute Doubly Differential Cross Sections for Production of Electrons in Ne<sup>+</sup>-Ne and Ar<sup>+</sup>-Ar Collisions

R. K. Cacak and T. Jorgensen, Jr.

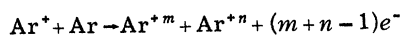
*Department of Physics, University of Nebraska, Lincoln, Nebraska 68508*

(Received 17 April 1970)

Absolute differential cross sections for the production of electrons by collisions of neon ions with a neon-gas target and argon ions with an argon-gas target were measured. The cross sections were doubly differential in angle and energy of the ejected electrons. The energy range of the primary ions was 50 to 300 keV. Electrons that were produced by the ion-atom collisions were analyzed in angle and energy, counted, and, from a knowledge of the other parameters of the apparatus, an absolute cross section was determined. The experimental results show some structure in the electron-energy spectra superimposed on a continuous background. This is consistent with the predictions of the Fano-Lichten electron-promotion model. Calculations based on the results of the Russek statistical model are compared with experiment.

### I. INTRODUCTION

Ionizing collisions of symmetric heavy ion-atom collisions of the type



are, in general, too complex to treat in a conventional quantum-mechanical manner, and other theoretical models have been proposed to explain some of the features of these collisions. Russek and his co-workers<sup>1</sup> have developed a statistical theory

that successfully predicts the probability of an ion appearing in a certain charge state after the collision as a function of other collisional parameters. Recently, Russek and Meli<sup>2</sup> have calculated the energy distribution of the electrons produced as a function of the energy transfer in a collision. These results were converted to cross sections by Bierman *et al.*<sup>3</sup> using the energy-transfer distributions of Everhart and Kessel<sup>4</sup> and empirical data relating the distance of closest approach to the energy transfer.<sup>5</sup> Bierman's calculations were compared to the energy spectrum of electrons from argon obtained earlier at this laboratory.<sup>6</sup> The